ADVANCED FUNCTIONAL MATERIALS
www.afm-journal.de

Search for Alternative Two-Step-Absorption Photoinitiators for 3D Laser Nanoprinting

*N. Maximilian Bojanowski, Aleksandra Vranic, Vincent Hahn, Pascal Rietz, Tobias Messer, Julian Brückel, Christopher Barner-Kowollik, Eva Blasco, Stefan Bräse, and Martin Wegener**

Recent studies have opened the door to a new generation of photoinitiators for 3D laser nanoprinting. Therein, the simultaneous absorption of two photons, commonly referred to as two-photon absorption, is replaced by the sequential absorption of two photons in two consecutive one-photon absorption processes. This process has been termed two-step absorption. Importantly, two-step absorption can be accomplished by inexpensive compact low-power continuous-wave blue laser diodes instead of femtosecond laser systems in the red spectral region. Red-shifting the second absorption step with respect to the first one results in an and-type optical nonlinearity based on two-color two-step absorption. Herein, alternatives are systematically explored to the few already reported one- and two-color two-step-absorption photoinitiators, including the search for photoinitiators that can be excited by one-color two-step absorption and be de-excited by a disparate laser color.

1. Introduction

A common approach to 3D laser printing of polymers is photopolymerization, where light solidifies a liquid photoresin. This resin contains mixtures of multifunctional monomers and photoinitiator molecules. The photoinitiator molecules absorb the light, generate free radicals, and subsequently start a radical chain polymerization. By scanning a diffraction-limited laser focus through the volume of the resin, 3D exposure patterns can be defined. The resin inherently requires an effective nonlinearity to suppress the tails of the laser focus that otherwise accumulate ("proximity effect") and prevent one from printing truly 3D objects.[1,2] In early experiments,[3] this nonlinearity has been provided in optical form by two-photon absorption,[4] which is determined by the imaginary part of the third-order nonlinear optical susceptibility.[5–7] Later, it has become clear that chemical nonlinearities can contribute as well, with[8] or without[9–12] optical nonlinearities. However, the vast majority of applications of 3D laser printing have been based on optical nonlinearities.[13–15]

High intensities of light are necessary to make optical nonlinearities efficient, which are commonly achieved by tightly focusing femtosecond or picosecond laser pulses.[2,16,17] Typically, ultrafast pulsed light sources are costly and large in

N. M. Bojanowski, V. Hahn, P. Rietz, T. Messer, M. Wegener
Institute of Applied Physics (APH)
Karlsruhe Institute of Technology (KIT)
76128 Karlsruhe, Germany
E-mail: martin.wegener@kit.edu

N. M. Bojanowski, V. Hahn, P. Rietz, C. Barner-Kowollik, E. Blasco, M. Wegener
Institute of Nanotechnology (INT)
Karlsruhe Institute of Technology (KIT)
76344 Eggenstein-Leopoldshafen, Germany

A. Vranic, J. Brückel, S. Bräse
Institute of Organic Chemistry (IOC)
Karlsruhe Institute of Technology (KIT)
Fritz-Haber-Weg 6, 76133 Karlsruhe, Germany

The ORCID identification number(s) for the author(s) of this article can be found under https://doi.org/10.1002/adfm.202212482.

DOI: 10.1002/adfm.202212482

C. Barner-Kowollik
Centre for Materials Science
School of Chemistry and Physics
Queensland University of Technology (QUT)
2 George Street, Brisbane, Queensland 4000, Australia

E. Blasco
Institute of Molecular Engineering Systems and Advanced Materials (IMSEAM)
Ruprecht-Karls-Universität Heidelberg
Im Neuenheimer Feld 225, 69120 Heidelberg, Germany

E. Blasco
Institute of Organic Chemistry (OCI)
Ruprecht-Karls-Universität Heidelberg
Im Neuenheimer Feld 270, 69120 Heidelberg, Germany

S. Bräse
Institute of Biological and Chemical Systems-Functional Molecular Systems (IBCS-FMS)
Karlsruhe Institute of Technology (KIT)
76133 Karlsruhe, Germany

volume, preventing further miniaturization of 3D laser nanoprinters and slowing the further spreading of this technology. Additionally, unwanted micro-explosions occur eventually when using intense femtosecond pulses in 3D laser printing.[18,19]

To overcome these issues, recent work suggested replacing two-photon absorption by two-step absorption.[20] This notion refers to a process in which a first photon is absorbed via one-photon absorption, leading to the population of some intermediate idle (triplet) state of the photoinitiator molecule after fast vibrational relaxation and intersystem crossing. The lifetime of this idle state can range from nanoseconds to milliseconds. Ideally, no chemical reaction of any sort is triggered from this energetically low-lying state. In the literature, such initiators are known as reluctant Norrish type I photoinitiators, e.g., a diketone such as benzil (BZ).[21] After absorption of a second photon, again via one-photon absorption, the electron is excited from the idle state to some higher excited (triplet) state, from which radicals are generated and radical polymerization is initiated. Excitation with one laser color for both transitions is possible if the ground-state absorption and the transient-absorption spectra overlap.[22] Under these conditions, the population of the upper excited electronic state (or exposure dose D) is proportional to the square of the local intensity of light, i.e., $D \propto I^2$, for both, two-step absorption and two-photon absorption.[20]

We note that for two-photon-absorption initiators, the two-photon-absorption cross section should be as large as possible, and the initiator should decay into radicals.[2] A decay from the triplet ground-state is not desired for two-step absorption initiators, because the overall process would be a one-photon-induced mechanism with a linear dependence of the dose on the intensity $D \propto I$.

When aiming to obtain luminescence rather than inducing polymerization, such two-step processes are known and commonly referred to as upconversion luminescence.[23] We avoid the term upconversion as it is also associated in a different context with nonlinear optical susceptibilities,[24] which two-step absorption is not. Mathematically, two-step absorption is rather described as the product of the imaginary parts of two linear optical susceptibilities.

The presented two-step absorption photoinitiators are, as most photoinitiators, ketones and hence contain a carbonyl group as their chromophore. For ketones, the visible absorption from the ground state to the first singlet excited state shows an $n\pi^*$-character, which leads to a fast intersystem crossing into an excited triplet state having $\pi\pi^*$ or intermixed $n\pi^*$–$\pi\pi^*$ character.[25] Fast internal conversion brings the system into the stable, lowest triplet state having a $n\pi^*$-character. Whereas ordinary initiators start the polymerization reaction via a bond-scission from the triplet ground-state (the Norrish type I reaction), this is not the case for two-step absorption photoinitiators. Here, the triplet ground-state energy is too low compared to the bond dissociation energy.[26] However, as for Norrish type II initiators, triplet-state ketones can alternatively also form radicals by abstracting hydrogen atoms from nearby susceptible groups.[27] As emphasized above, such a reaction leads to an undesired one-photon-triggered polymerization reaction, hence a linear dependence of the cross-linking density on the intensity. The lacking nonlinearity results in a large proximity effect. Therefore, side reactions, like hydrogen atom abstraction, from triplet ground-state need to be suppressed, e.g., by employing scavenger molecules.[28,29] Two-step absorption has been demonstrated experimentally in single-color form[20] as well as in two-color form,[30] where the ground and intermediate state contain non-overlapping regions, avoiding that light of either wavelength can excite both transitions.[31] However, the number of functioning photoinitiators and corresponding resins based on two-step absorption is extremely small (currently three published—two based on diketones)[20,30,32] compared to hundreds of different photoinitiators for two-photon absorption.

2. Results and Discussion

2.1. Photoinitiators, Resin Composition, and Printability

This article discusses 22 potential alternative photoinitiators for 3D laser printing based on two-step absorption (**Figure 1**). Possible photoinitiator system modifications compared to BZ and biacetyl (BA) include electron-rich 5-membered or electron-poor 6-membered heterocyclic rings by introducing heteroatoms (N, S, and O) resulting in pyridil (PYR), thenil (TN), and furil (FUR), respectively. To induce a bathochromic shift, we introduce nitro-groups resulting in *p*- and *m*-dinitrobenzil (NBZ), or substitute phenyl by naphthyl to 1- and 2-naphthil (NT), increasing the aromatic system. Introducing methyl groups should decrease the overall reactivity of the radical polymerization initiation,[33] thereby increasing the laser threshold power for polymerization. Previously, for fluorine-substituted benzil, an increased radical reactivity compared to unsubstituted benzil was observed.[34,35] Therefore, we investigate *p*-dimethylbenzil (Me_2BZ) and *p*-difluorobenzil (F_2BZ). Influences on solvation are expected from introducing additional carboxyl (CBZ and DCBZ) and hydroxy groups (HBZ). We increase the conjugation length via additional diketones for bisbenzil (BBZ) and thus double the number of reactive sites forming radicals.

Inductive effects should also account for hexanedione (HD) with an increased alkyl chain length. Furthermore, we investigate a structural combination of BZ and BA, namely 1-phenyl-1,2-propandione (PPD). Additionally, the closely related tetraphenyl bisimine (TPBI), as *N*-analogous to carbonyls, is tested as an initiator. As a third class, we introduce rotation-restricted diketones, based on ortho-substitution leading to steric hindrance, e.g., 2,4,6-trimethylbenzil (MesBZ), 2,2′-6,6′-tetramethylbenzil (Me_4BZ) or cyclic diketones as camphorquinone (CQ) or 3,3,-5,5-tetramethylcyclopentadione (Me_4CPD).

Out of these, 12 have been synthesized via several routes. Synthetic procedures can be found in the Supporting Information. 1-NT, Me_4BZ, and TN are obtained via a direct synthetic route to diketones reacting a Grignard reagent with oxalyl chloride.[36] 2-NT, PYR, and FUR are synthesized by oxidation of the corresponding benzoins. 2-NT can easily be oxidized using 1,8-diazabicyclo[5.4.0]undec-7-en for deprotonation under ambient conditions,[37] whereas FUR and PYR need harsher conditions employing Corey–Suggs reagent or nitric acid.[38,39] Nitrobenzils *m*- and *p*-NB, CBZ, and HBZ are synthesized from corresponding symmetric diarylacetylenes by oxidation.[40–43] The bisimine is synthesized via an aldimine coupling reaction.[44] Finally, Me_4CPD is furnished from the oxidation of the

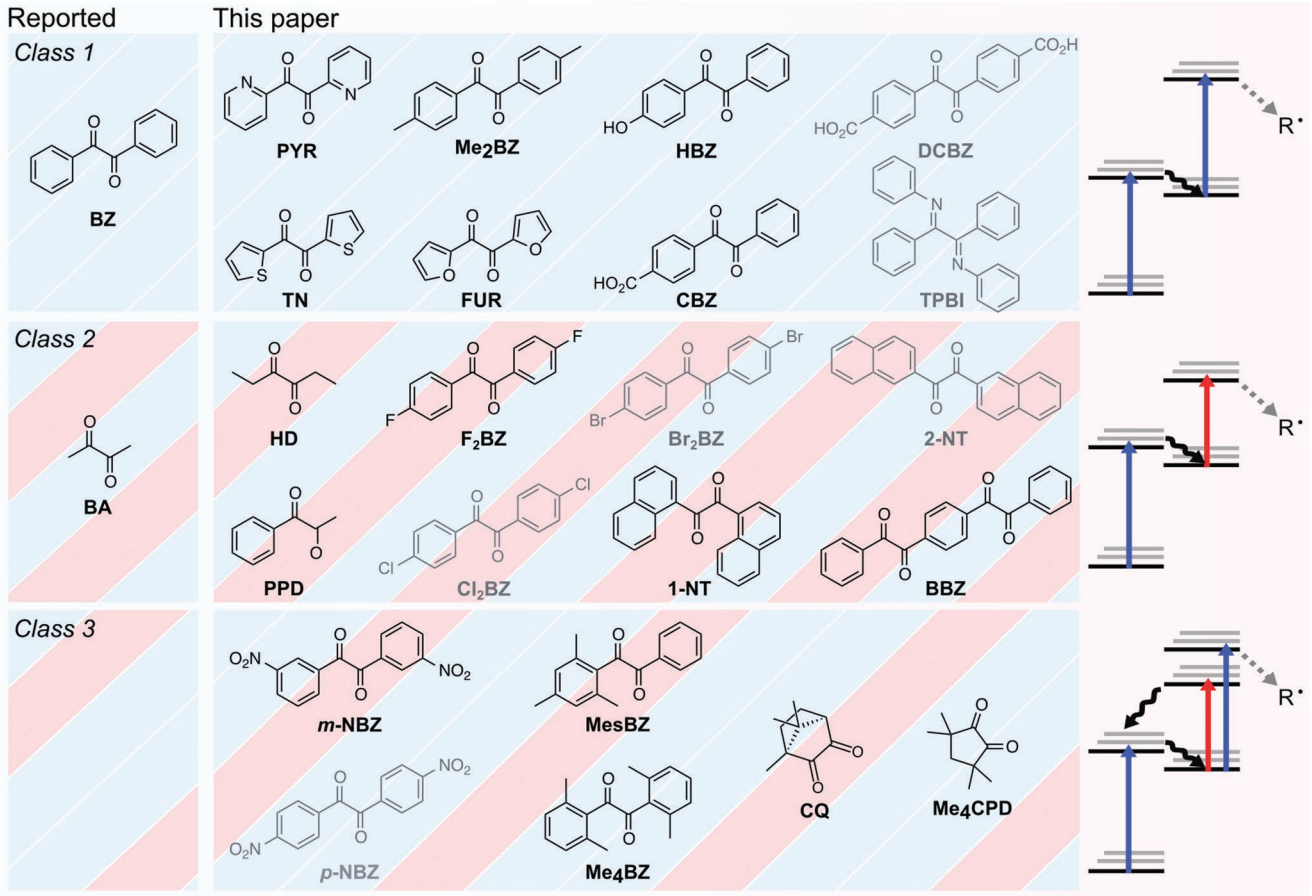

Figure 1. Two-step absorption photoinitiator diketone compounds investigated within this publication. Benzil (BZ) and biacetyl (BA) were previously reported as initiators in 3D laser printing based on two-step absorption. In this publication, 22 additional diketones are investigated. They are assigned to three classes: one-color two-step absorption, two-color two-step absorption, and one-color two-step absorption combined with a depletion process. The color scheme represents the laser wavelengths used in the characterization experiments: blue for 405 nm and red for 640 nm. Energy-level diagrams represent one-color two-step absorption, two-color two-step absorption, and one-color two-step absorption combined with a depletion mechanism. Grey-marked initiators are insoluble (DCBZ, Cl_2BZ, Br_2BZ, and *p*-NBZ) or show no reaction to light at 405 nm (TPBI and 2-NT).

corresponding commercially available monoketone employing selenium dioxide.[45]

Some basic requirements must be considered, too. Ideally, the initiator should be well soluble in the pure monomer, otherwise strong shrinkage will occur after development.[46] Cl_2BZ, Br_2BZ, DCBZ, and *p*-NBZ are insoluble in the acrylic monomers used in this work and hence not considered in the printing experiments. 2-NT is well soluble in acrylates but exhibits negligible ground-state absorption >353 nm due to a hypsochromic shift.[47] 2-NT is therefore excluded. TPBI has shown no reaction to light at 405 nm and is therefore also not further considered in what follows. We group the remaining 18 initiators including BZ and BA into three different classes (Figure 1): one-color two-step absorption (seven molecules), two-color two-step absorption (six molecules), and one-color two-step absorption combined with a depletion process (five molecules). We note that no molecules exhibiting two-step absorption combined with a depletion process (third class) have been reported previously. Each one of these 18 initiator molecules is combined in a photoresin with pentaerythritol triacrylate (PETA) as a monomer and 2,2,6,6-tetramethylpiperidinyloxyl (TEMPO) as a scavenger. TEMPO, being a persistent radical,[48,49] can suppress undesired hydrogen abstraction by recombination. In addition, it lowers the lifetime of the intermediate T_1 state.[29] The concentrations for initiators are 100 mm (25 mm for 1-NT due to low solubility) and 50 mm (respectively, 12.5 mm) for TEMPO. In what follows, we name the resins using the abbreviations for the initiators as introduced above.

To evaluate the printability of our resins, we performed point-exposure experiments to investigate the dependence of threshold laser power on the exposure time t_{exp}. For each exposure time, we determine the blue laser threshold power $P = P_{405}$ that leads to a polymerized dot that is visible in an optical microscope after the development of the sample in acetone and isopropanol (a detailed description is given in the Supporting Information). In **Figure 2**a, we plot P_{405} versus t_{exp} on a double-logarithmic scale for FUR and BBZ (blue and red dots, respectively). The straight lines with the indicated slopes are guides to the eye. For low powers, the data show a slope close to – 1/2, corresponding to a behavior $P_{405} \propto 1/t_{exp}^{1/2}$. For higher powers, the data rather follow a slope of – 1, corresponding to a dependence $P_{405} \propto 1/t_{exp}$. This behavior is consistent with the rate-equation

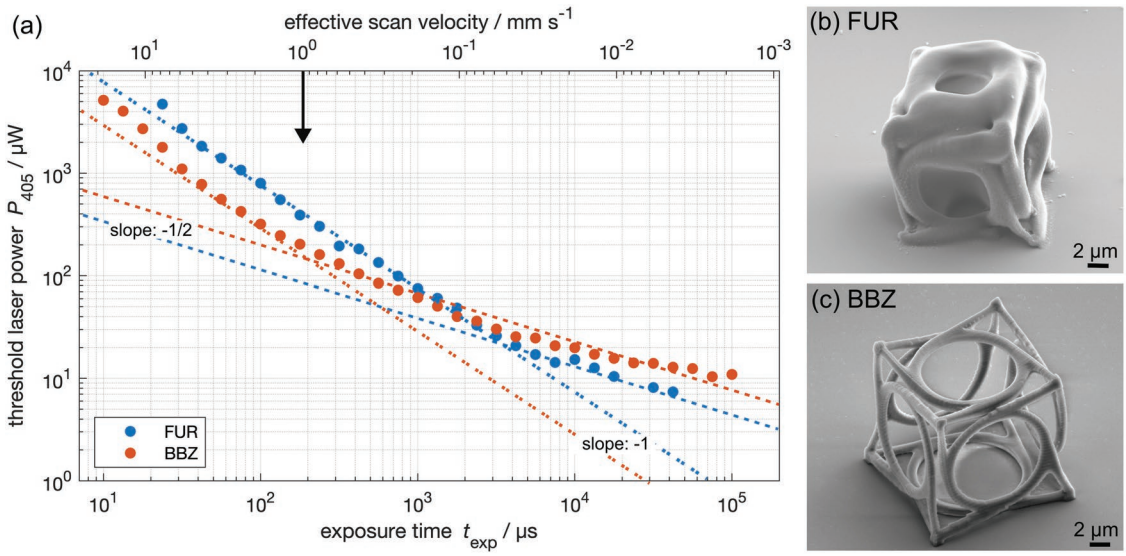

Figure 2. Exemplary evaluation of printability for FUR and BBZ. a) Measured threshold laser power versus exposure time (lower horizontal scale) after point exposure experiments. On the upper horizontal scale, the exposure time is converted into an effective focus velocity. Blue dots represent printing results from FUR as an initiator, and red dots represent printing experiments of BBZ. The dashed straight lines with the indicated slopes serve as guides to the eye. b) Oblique view electron micrograph of one unit-cell of a chiral metamaterial printed at a power of P_{405} = 226 µW and at a focus speed of v = 1 mm s^{-1}. FUR is used as an initiator. c) The same structure, printed at a power of P_{405} = 42 µW but for BBZ instead of FUR.

expectation for two-step absorption.[20] In addition, we printed a single unit cell of a chiral metamaterial[50] by focusing the laser beam using an oil-immersion microscope objective lens with a numerical aperture of NA = 1.4 through the glass substrate into the resin and scanning the laser focus at a speed of 1 mm/s.

In Figure 2, the evaluation of printability is exemplarily shown for FUR and BBZ. For FUR (see Figure 2b), we find very bad sample quality, which we attribute to a pronounced proximity effect. This assessment is consistent with the fact that the FUR data in Figure 2a (blue dots) correspond to a slope of − 1 under these conditions. The electronic structure change when going from BZ to FUR mainly leads to reduced C−C bond stability. We interpret that the reduced stability enables the generation of radicals from T_1, resulting in a pronounced proximity effect. In contrast, for BBZ (red dots) under the same conditions, we find good quality of the printed sample shown in Figure 2c. This finding is consistent with the fact that the BBZ data in Figure 2a (red dots) correspond to a slope of − 1/2 at a scan velocity of 1 mm/s (black arrow).

Let us now turn our attention to molecules covered in Figure 1 and not covered in Figure 2. All initiators, including the ones in classes two and three, are tested for printability via one-color two-step absorption. For PYR, the overall threshold needed for printing single dots is larger by one order of magnitude compared to BZ, despite a similar ground-state extinction coefficient (see Figure S2, Supporting Information). We attribute the formation of intramolecular chalcogen-bonds to limit the printability of TN.[51] Additionally, we cannot exclude low transient absorption at 405 nm. The same holds true for CQ,[31] which normally acts as a Norrish type II initiator proceeding via hydrogen abstraction,[52] a mechanism that is suppressed by the scavenger. Polymerization of the resin 1-NT needs overall higher powers (Figure S6, Supporting Information), caused by the limited photoinitiator solubility and hence low photoinitiator concentration. Furthermore, solely a linear temporal dependence of the threshold is observed, disqualifying this initiator for one-color two-step 3D printing. Polymerization of MesBZ and Me_4BZ requires an increased overall threshold power compared to BZ (Figure S7, Supporting Information). We attribute this to the formed radicals, which are sterically hindered and therefore possess higher stability and reduced initiation reactivity. For methyl- and fluorine-substituted benzils, we do not observe a change in reactivity (Figure S5,S6, Supporting Information).

In our introduction, we mentioned the relevance of chemical nonlinearities in addition to optical nonlinearities. In the point-exposure experiments, such nonlinearities lead to a near-constant polymerization threshold power (i.e., a high apparent nonlinearity) for long exposure times. This chemical nonlinearity is typical for oxygen quenching of triplet states and inhibition of radicals formed (see Figures S5,S7, Supporting Information).[8,53,54] For higher laser powers, oxygen concentration within the focal volume can be depleted, whereas for low laser powers and long exposure times oxygen diffusion into the volume occurs at similar rates as polymerization initiation.[53] For *m*-NBZ, CBZ, and, HBZ, this so-called Schwarzschild effect[55] is more pronounced compared to all other initiators. We interpret this behavior as being due to the limited re-diffusion of initiators by increased electrostatic forces of attraction, i.e., to hydrogen bonding.

In Figure S8 (Supporting Information), we present a gallery of electron micrographs of one-color 3D-printed metamaterial unit cells for the remaining 11 initiators (out of all classes) not already covered in Figure 2 or later herein. For most 3D-printed structures, staircasing effects caused by the hatching and slicing are pronounced, indicating a high resolution. For Me_4BZ, the

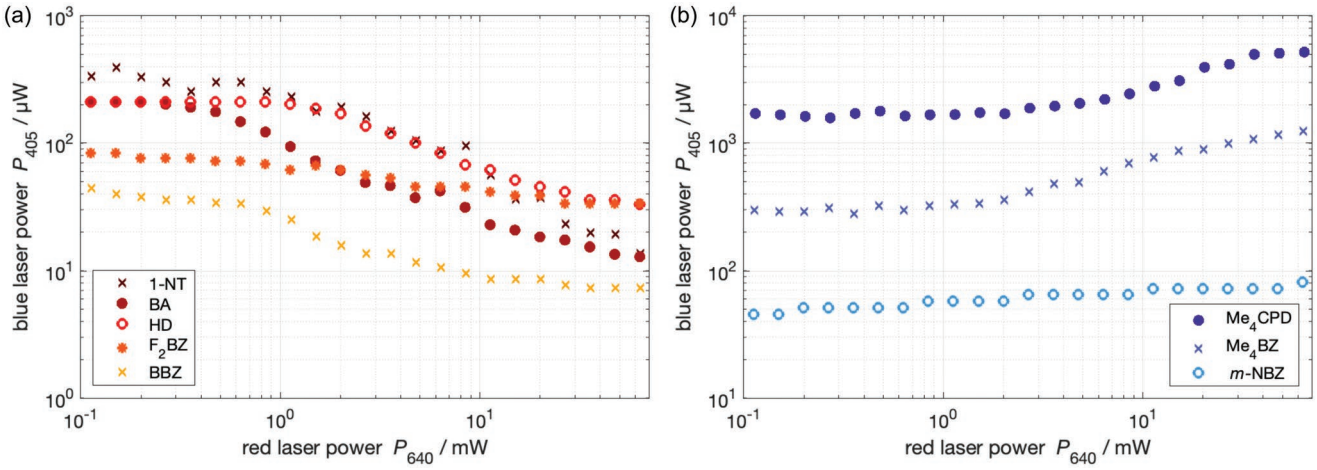

Figure 3. Two-color polymerization-threshold diagram for selected two-step absorption photoinitiators for a fixed scan velocity. a) The initiators BA, HD, F_2BZ, BBz, and 1-NT show a decrease in the blue threshold power for increasing red laser power. b) The initiators *m*-NBZ, Me_4BZ, and Me_4CPD show an increase in the blue threshold power for increasing red laser power.

structural fidelity is low. We attribute this behavior to a small nonlinear exponent in the scaling of the local exposure dose $D \propto P_{405}^N$ with $N < 1.6$ (Figure S7, Supporting Information). A low nonlinearity of $\approx N = 1$ is similarly apparent in the printing of the unit cell from the CBZ and PYR resins compared to the FUR resin. For the PYR resin, we have reduced the printing speed to 500 µm/s. We attribute this increased proximity effect to an extended intermediate-state lifetime, which can be explained by the strong electron-withdrawing groups, such as the nitrogen of pyridyl ketones, that stabilize the $n\pi^*$ triplets.[25] For the two-color two-step initiators in Figure 1, printing is also possible with a single excitation wavelength of 405 nm at sufficiently larger laser powers. BBZ and HD show better one-color printability than BA.

2.2. Two-Color Two-Step Absorption and Two-Step Absorption and Depletion

We have investigated the two-color two-step behavior of all soluble initiators shown in Figure 1 by co-focusing two laser beams of wavelengths λ_1 = 405 nm (blue) and λ_2 = 640 nm (red) to spatially overlapping ordinary Gaussian foci. We print dashed lines at a constant scan velocity of v = 100 µm/s and variable laser powers (compare Figure S10, Supporting Information). For each red laser power P_{640}, we determine the minimal blue laser threshold power P_{405} that leads to a polymerized line visible in a dark-field optical microscope image. The blue laser power and the corresponding power for the red laser are summarized in a double logarithmic plot of the blue laser power against the red laser power in **Figure 3**.

We find two behaviors that are the polar opposite of each other. First, for two-color two-step polymerization as described previously,[30] the blue laser polymerization threshold decreases in a sigmoid fashion versus red laser power. This behavior leads to a logical AND-type optical nonlinearity: Under a deliberate choice of blue and red laser power, both lasers must be switched on to generate radicals for polymerization (Figure 1b). Consequently, it is not possible to produce, e.g., satisfactory 3D printing results employing BA as a one-color two-step initiator (cf. previous section). BA as an initiator has shown promising results in light-sheet 3D microprinting.[30] However, the initiator concentration of uncapped samples decreases due to BA evaporation out of the resist, caused by BA's high vapor pressure. As an alternative, we found further initiators grouped in class two in the overview (Figure 1). HD shows a sigmoidal curve shifted toward higher red laser powers and allows writing with only the blue laser color. The behavior of 1-phenylpropan-1,2-dione (PPD) is between those of BA and BBZ (Figure S9, Supporting Information). PPD shows a lowering of the blue threshold power for high red laser powers (P > 10 mW) and allows for good printability in the one-color two-step mode.

Not only alkyl-substituted diketones show such a two-color two-step absorption process. Non-aromatic diketones have a strongly blueshifted transient absorption spectrum.[22,31] Therefore, the overlap between the ground-state and the excited-state absorption spectra is negligibly small.[31] Aromatic compounds bathochromically shifting the spectra compared to BZ should lead to a two-color two-step behavior, too. 1-NT shows limited printability using one-color two-step absorption (not shown) and might be—with other solubility-mediating side groups—a promising candidate for a two-color two-step initiator. BBZ has an extended π-system (carbonyl-based electron-conjugated effect) and shows a behavior similar to BA. The effect of fluorine groups on benzil is less clear. Fluorine can extend conjugation by its back-donation of nonbonding electrons to the aromatic π-system.[56] Additionally, we assume transitions from low triplet states with mixed character ($n\pi^*$ and $\pi\pi^*$) to higher triplet states with $\pi\pi^*$ character.[25] This effect of intermixed triplet states is expected to be less pronounced for Me_2BZ. As shown in Figure S9 (Supporting Information), the blue threshold power only decreases by a factor of two with increasing red laser power. Hence, we do not consider this molecule as a promising two-color two-step initiator and order it to class one (Figure 1). We conclude, that extending the conjugated π-system compared to BZ is the predominant reason for

the two-color two-step behavior of aromatic systems, most likely induced by a red-shift of the excited-state absorption spectrum.

Let us now turn to the second, polar opposite behavior of two-color two-step initiators as summarized in Figure 3b. With increasing red laser power, we find a monotonous increase of the blue threshold laser power from 42 to 80 μW for *m*-NBZ. This behavior indicates one-color two-step absorption combined with a depletion mechanism induced by the red laser light. Different depletion pathways can explain this behavior. For instance, the red laser could induce optical transitions from the lowest triplet state to some higher triplet state, from where reverse-intersystem crossing brings the molecule back to its higher excited singlet state followed by non-radiative relaxation. To further clarify the nature of the depletion mechanism, we have investigated the sterically hindered photoinitiators Me_4BZ and MesBZ. Steric hindrance refers to the influence of the spatial extent of the methyl groups and limits the rotation around the intercarbonyl dihedral angle ϕ_{CO-CO}. MesBZ possesses sterical hindrance just on only one aromatic ring and serves as a reference. Me_4BZ shows an increase of the blue laser threshold power from 300 μW to beyond 1 mW upon increasing the red laser power from 57 μW to 65 mW (see Figure 3b). In contrast to the latter case of two-color two-step absorption, a flatter sigmoid curve shape is observed. This step-like fashion contrasts with the linear increase for *m*-NBZ. Two-fold substitution for sufficient hindrance of rotation around the intercarbonyl dihedral angle is needed. While Me_4BZ shows promising results in depletion experiments, the overall printability using 405 nm is limited (cf. Figure S8, Supporting Information).

Rotational restriction can be ensured by introducing cyclic diketones, too.[57] Here, the diketone is enforced cisoid (with an intercarbonyl angle $\phi_{CO-CO} = 0°$) in all states. Resins composed of CQ as a Norrish type II initiator, as such a bicyclic molecule, are not printable. We argue that radicals formed by homolytic bond scission do not separate and recombine easily. The monocyclic initiator Me_4CPD shows a pronounced depletion effect. Here, the blue laser threshold power increases by a factor of >3 to up to 5 mW blue laser power needed to write lines (see Figure 3). As the formed radicals are still covalently linked, radical recombination is a possible explanation for the overall higher threshold compared to other initiators such as BZ.

The relevant states of a depletable photoinitiator molecule are schematically shown in Figure 1. We exclude stimulated-emission depletion (STED)[58–62] as the governing mechanism since the fluorescence quantum yield of the investigated initiators is <1%.[63] We rather consider a competing two-step absorption mechanism from T_1 to a triplet state T_m,[65] that can be populated by excitation with a second wavelength (nominal $\lambda_2 = 640$ nm). A higher triplet state T_n can be populated by the absorption of photons with $\lambda_1 = 405$ nm, possessing higher energy to suppress the depletion mechanism and leading instead to the cleavage of the dicarbonyl bond, representing one-color two-step absorption.

Most of the literature argues that the nature of the lowest triplet state strongly depends on the intercarbonyl dihedral angle ϕ_{CO-CO}.[63–66] Steric hindrance also freezes the ground-state conformation for the triplet state, preventing a rotation around the intercarbonyl dihedral angle.[64] In general, the introduction of coplanarity will increase the energy of the ground state relative to that of the excited state, and the corresponding transient absorption will occur at longer wavelengths.[63,66]

Both the coplanarity of the carbonyl groups and the ring constraints enhance the electron acceptor character of the diketones toward radical scavengers, generally characterized by hydrogen and electron donor character. Additionally, the energy of the triplet state T_m singlet is expected to be close to excited state energies, facilitating the reverse intersystem crossing. Therefore, the depletion mechanism can be explained as the combination of these two effects.

2.3. Two-Step Absorption and Depletion of a Cyclic Diketone

Our interest in depletable one-color two-step initiators arises from the fact that depletion opens a conceptual pathway to overcoming the diffraction barrier.[61,62,67,68] Therefore, we have further investigated Me_4CPD. We have printed a single unit cell of a chiral metamaterial and a #3DBenchy structure, employing one-color two-step absorption without depletion (**Figure 4**a,b). Next, we perform depletion experiments in which the Gaussian focus of a red laser is located at the same position as the Gaussian focus of a blue laser. To test the reversibility of the depletion process, we write a loop pattern. In Figure 4c–e, the blue laser (405 nm wavelength) is switched on all the time whereas the red laser (640 nm wavelength) is switched on only in the central part. Reversibility is confirmed by the following observations. First, previously written lines are not damaged or modified by the depletion laser at the used laser power. Second, it is possible to write in a region that has previously been depleted by the depletion laser.

The polymerization can be suppressed completely if the blue and red laser powers are chosen adequately. For example, in Figure 4e, to obtain complete depletion, we have chosen $P_{405} = 672$ μW for the blue laser power, and $P_{640} = 25$ mW for the red laser power. Complete depletion can no longer be achieved for $P_{640} = 12.5$ mW. Likewise, depletion also becomes incomplete (disrupted lined), if we further increase the blue laser power by a few percent (not depicted). This overall behavior is expected for any depletable initiator.

For **Figure 5**, we combine the depletion process with a special focus for the red depletion laser beam. This special focus is achieved by introducing a home-built phase mask into the beam path of the red laser.[58] This dielectric mask phase- shifts one half of the depletion beam wave front by π with respect to the other half of the wave front. The phase profile leads to the intensity distribution in the focal plane shown in the lower part of Figure 5a with a line of zero intensity through its middle. This laser focus as well as the blue Gaussian focus (see top of Figure 5a) were measured and aligned with respect to each other by scanning an 80 nm diameter gold bead embedded in a polymer matrix through the focus while recording the back-scattered light. A set of lines is written with a fixed blue excitation laser power of $P_{405} = 616$ μW, whereas the depletion laser is switched on and off during the writing process as schematically illustrated in the bottom panel of Figure 5b. From line to line, from bottom to top, the depletion laser power increases.

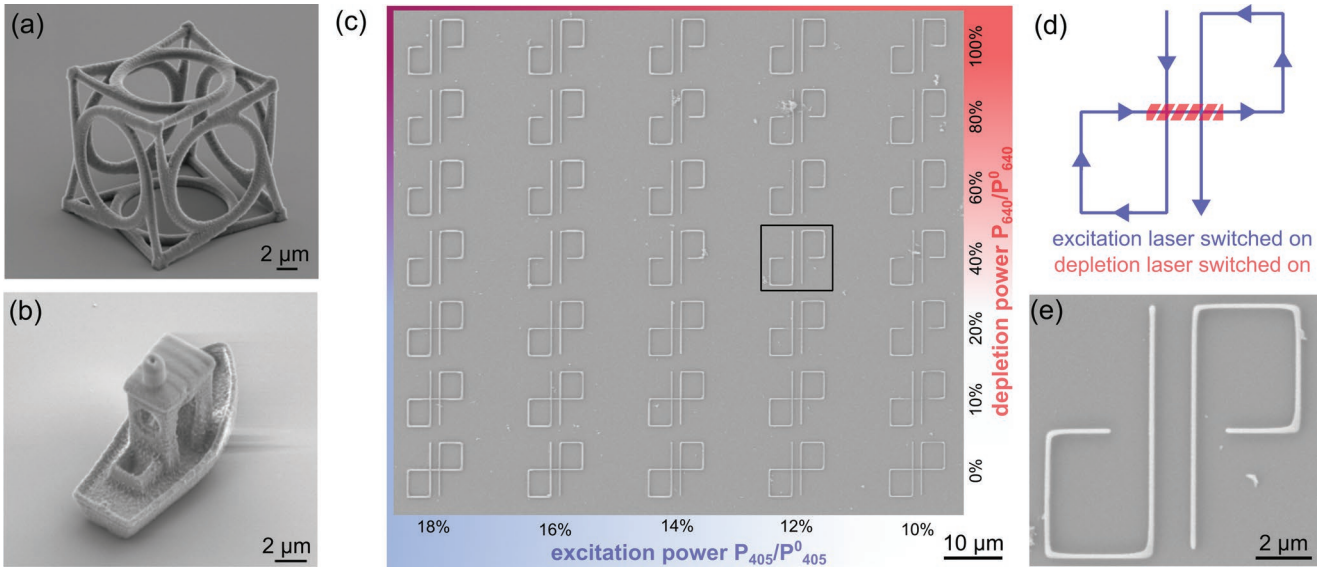

Figure 4. Gallery of electron micrographs printed using structures with the depletable initiator Me_4CPD. a) Oblique-view electron micrograph of a single chiral metamaterial unit cell laser-printed at a power of $P_{405} = 1.86$ mW and at a focus speed of $v = 500$ µm s^{-1}. b) Same, but for a laser-printed #3DBenchy structure at $P_{405} = 2.7$ mW and at a focus speed of $v = 1$ mm s^{-1}. c) Top-view electron micrograph of an array of loops printed by local excitation with a spatially overlapping second Gaussian laser beam. The blue excitation power ($P^0_{405} = 5.6$ mW) increases from right to left, and the depletion power ($P^0_{640} = 62.3$ mW) increases from bottom to top. d) Scheme of the writing pattern used in (c) illustrating for that parts the depletion laser has been switched on. e) Magnified view of one of the patterns in (c) revealing the reversibility of depletion. Previously written lines are not altered by the depletion laser, and it is possible to write in a region that has previously been depleted.

The minimum full-width-at-half-maximum (FWHM) of the averaged line profile, obtained by averaging the data from the scanning electron micrographs along the line axis, is ≈100 nm for zero depletion-laser power and decreases by about a factor of two to a FWHM of ≈50 nm, albeit with partly collapsing and breaking-up lines (see the upmost row in Figure 5b).

While the overall results are highly encouraging in terms of convincingly showing reversible depletion by the red laser combined with a one-color two-step absorption process for the excitation at 405 nm, we emphasize that these results do not yet provide evidence for improved resolution in the sense of minimum achievable distance between adjacent lines. Furthermore, the real challenge lies in applying reversible depletion to 3D printing by using, for example, bottle-beam foci of light. Such experiments are demanding,[62] but are part of our future plans.

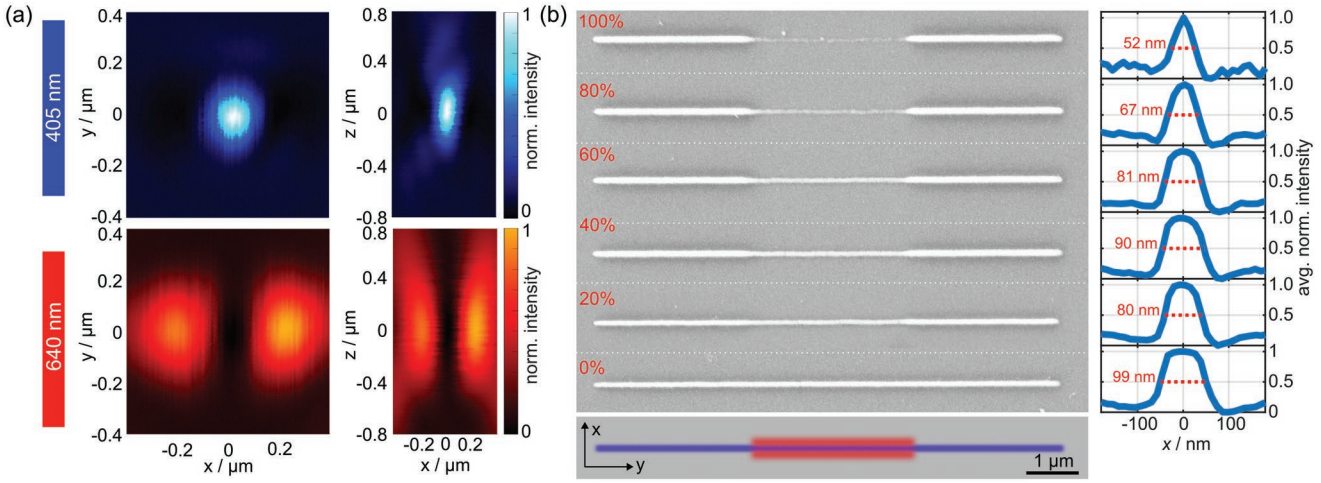

Figure 5. Depletion experiments using co-focused excitation beam and depletion beam with a phase mask. a) False-color plots of laser focus point-spread functions measured by scanning gold beads through the foci and recording the backscattered light. Cuts within the *x*–*y* and *x*–*z* planes are depicted. b) Top-view electron micrograph of a set of lines for that the depletion laser is switched on in the center of lines (see scheme at the bottom). The linewidths become smaller with increasing depletion laser power. On the right-hand side, we show extracted line profiles obtained by averaging along the axis of the depleted line.

3. Conclusion

We investigated 22 novel initiators as candidates in resists for two-step absorption 3D laser printing. Out of these 24 including BZ and BA, eight were not soluble or printable at all, seven including MesBZ work as one-color two-step photoinitiators at 405 nm wavelength, 6 initiators function as two-color two-step photoinitiators, and three act as one-color two-step photoinitiators that can be depleted by a second continuous-wave laser operating at a different color. Printability is evaluated by point-exposure experiments and exemplary 3D printed structures. Ground-state absorption is dominated by absorption within the diketone moieties, whereas excited-state absorption is influenced by the substitution or conjugation of substituents. We conclude that for the two-color two-step absorption mechanism not only alkyl groups are suitable as substitution patterns of diketones (as in BA and HD), but also larger conjugation of a bathochromic-shifted, aromatic system supports such a mechanism. The triplet-state energies are additionally influenced by the trans/cis conformation and by the degree of conjugation of the carbonyl groups with their adjacent phenyl moieties. The perhaps most interesting aspect of our work regarding future possibilities is that rotationally locked diketones open the door to depletable two-step absorption initiators. On this basis, inexpensive and compact setups based on continuous-wave lasers come into reach that systematically break the optical diffraction barrier in 3D laser printing.

4. Experimental Section

3D Printing Setup: The 3D printing setup (405 nm excitation wavelength for one-color two-step nanoprinting) was described in full detail elsewhere.[20] Additionally, for depletion experiments, the blue laser was combined with the collimated beam of a 640 nm nominal wavelength fiber-coupled laser (PhoxXplus 638-150, Omikron) by a dichroic mirror (DMLP567, Thorlabs GmbH). The laser foci were superimposed in the focal plane and characterized with scattered light of gold beads (80 nm nominal diameter) dispersed on a glass coverslip.[58] All laser power values quoted in the paper were measured at the entrance pupil of the objective lens using a semiconductor sensor (TP86, Coherent).

Substrates: The resin was contained in a polydimethylsiloxane (Sylgard 184 silicone elastomer) ring ($d = 5$ mm) placed on a methacrylate silanized glass coverslip (no. 1.5H, Paul Marienfeld. The substrates were cleaned in a 4 vol% solution of Hellmanex III (Hellma GmbH & Co KG) and functionalized with 3-(trimethoxysilyl)propyl methacrylate (Merck KGaA).

Sample Development: All printed samples were developed by immersing the sample for 3 min. in a bath of acetone and 2-propanol (UV/IR grade). The samples were then blow-dried in a gentle stream of nitrogen.

Photoresin Composition and Synthesis: The initiators BZ, BA, HD, PPD, BBZ, and CQ, as well as the monomer PETA and TEMPO were purchased from Sigma-Aldrich. Halogenated derivatives of benzil (F_2BZ, Cl_2BZ, and Br_2BZ) were purchased from TCI Chemicals. All chemicals were used without further purification. MesBZ was thankfully provided by Elena Frick and synthetic procedures were published elsewhere.[34] Synthetic work for PYR, TN, FUR, CBZ, DCBZ, HBZ, 1-, and 2-NT, *m*- and *p*-NT, Me_4BZ, and Me_4CPD was further described in the Supporting Information.

The different photoresin systems were named accordingly to the abbreviations for the initiators. All initiators (100 mm, except 25 mm for 1-NT) and TEMPO (50 mM, except 12.5 mm for 1-NT) were dissolved in PETA. The mixture was stirred at 45 °C until all the compounds were dissolved.

Scanning Electron Microscopy (SEM): SEM of all fabricated structures was performed with a Zeiss SURPA 55VP (Carl Zeiss AG) at a primary electron energy of 5 kV.

Extinction and NMR Spectra: The extinction spectra were recorded in spectroscopy-grade acetonitrile in a quartz cuvette using a Cary 100 or 300 (Agilent Technologies) spectrometer.

^{1}H NMR and ^{13}C NMR spectra were recorded in $CDCl_3$ or deuterated DMSO-d_6 at room temperature on a Bruker Avance III (500 MHz). Chemical shifts were reported in δ units relative to the solvent residual peak ($CHCl_3$ in $CDCl_3$ at $\delta = 7.27$ ppm, respectively, $\delta = 77.0$ ppm or DMSO-d_5 in DMSO-d_6 at $\delta = 2.50$ ppm, respectively, $\delta = 39.5$ ppm). The following abbreviations were used to indicate the signal multiplicity: s (singlet), d (doublet), t (triplet), or m (multiplet). Coupling constants (J) were given in Hz and refer to H,H-couplings. All NMR spectra were integrated and processed using Mestrenova.

Supporting Information

Supporting Information is available from the Wiley Online Library or from the author.

Acknowledgements

The authors thank Anna Mauri, Mariana Kozlowska, and Wolfgang Wenzel (all KIT) for stimulating discussions and for a thorough reading of this manuscript. The authors acknowledge funding by the Deutsche Forschungsgemeinschaft (DFG) through the Excellence Cluster "3D Matter Made to Order" (EXC-2082/1-390761711), the Carl Zeiss Foundation through the "Carl-Zeiss-Foundation-Focus@HEiKA", the Helmholtz Association through the Helmholtz program "Materials Systems Engineering (MSE)", and the Max-Planck School of Photonics. We further acknowledge support from the Karlsruhe School of Optics & Photonics (KSOP). C.B.-K. acknowledges the Australian Research Council (ARC) for funding in the context of a Laureate Fellowship, enabling his photochemical research program.

Open access funding enabled and organized by Projekt DEAL.

Conflict of Interest

The authors declare no conflict of interest.

Author Contributions

N.M.B., A.V., and V.H. performed all printing experiments within this manuscript. N.M.B., A.V., and J.B. synthesized initiators. N.M.B., V.H., T.M., and P.R. performed initial experiments on two-step absorption initiators. N.M.B. and M.W. drafted an initial version of the manuscript. M.W. and S.B. supervised the effort. All authors contributed to the interpretation of the results and to the writing of the manuscript.

Data Availability Statement

The data that support the findings of this study are openly available in KIT Open at https://doi.org/10.5445/IR/1000152770, reference number 1000152770.

Keywords

3D laser nanoprinting, photoinitiators, two-photon absorption, two-step absorption

Received: October 27, 2022
Revised: November 16, 2022
Published online:

[1] C. Arnoux, L. A. Pérez-Covarrubias, A. Khaldi, Q. Carlier, P. L. Baldeck, K. Heggarty, A. Banyasz, C. Monnereau, *Addit. Manuf.* **2022**, *49*, 102491.
[2] P. Kiefer, V. Hahn, M. Nardi, L. Yang, E. Blasco, C. Barner-Kowollik, M. Wegener, *Adv. Opt. Mater.* **2020**, *8*, 2000895.
[3] O. N. S. K. S. Maruo, *Opt. Lett.* **1997**, *22*, 132.
[4] M. Göppert-Mayer, *Ann. Phys.* **1931**, *401*, 273.
[5] M. G. Kuzyk, C. W. Dirk, *Phys. Rev. A* **1990**, *41*, 5098.
[6] C. W. Dirk, L. -T. Cheng, M. G. Kuzyk, *Int. J. Quantum Chem.* **1992**, *43*, 27.
[7] T. R. Ensley, H. Hu, M. Reichert, M. R. Ferdinandus, D. Peceli, J. M. Hales, J. W. Perry, Z. Li, S.-H. Jang, A. K.-Y. Jen, S. R. Marder, D. J. Hagan, E. W. Van Stryland, *J. Opt. Soc. Am. B* **2016**, *33*, 780.
[8] J. B. Mueller, J. Fischer, F. Mayer, M. Kadic, M. Wegener, *Adv. Mater.* **2014**, *26*, 6566.
[9] P. Mueller, M. Thiel, M. Wegener, *Opt. Lett.* **2014**, *39*, 6847.
[10] M. T. Do, T. T. N. Nguyen, Q. Li, H. Benisty, I. Ledoux-Rak, N. D. Lai, *Opt. Express* **2013**, *21*, 20964.
[11] P. Delrot, D. Loterie, D. Psaltis, C. Moser, *Opt. Express* **2018**, *26*, 1766.
[12] M. Thiel, J. Fischer, G. Von Freymann, M. Wegener, *Appl. Phys. Lett.* **2010**, *97*, 221102.
[13] T. Gissibl, S. Thiele, A. Herkommer, H. Giessen, *Nat. Photonics* **2016**, *10*, 554.
[14] M. A. Wolff, F. Beutel, J. Schütte, H. Gehring, M. Häußler, W. Pernice, C. Schuck, *Appl. Phys. Lett.* **2021**, *118*, 154004.
[15] M. Farsari, B. N. Chichkov, *Nat. Photonics* **2009**, *3*, 450.
[16] K. J. Schafer, J. M. Hales, M. Balu, K. D. Belfield, E. W. Van Stryland, D. J. Hagan, *J. Photochem. Photobiol., A* **2004**, *162*, 497.
[17] E. Skliutas, M. Lebedevaite, E. Kabouraki, T. Baldacchini, J. Ostrauskaite, M. Vamvakaki, M. Farsari, S. Juodkazis, M. Malinauskas, *Nanophotonics* **2021**, *10*, 1211.
[18] J. Fischer, J. B. Mueller, J. Kaschke, T. J. A. Wolf, A.-N. Unterreiner, M. Wegener, *Opt. Express* **2013**, *21*, 26244.
[19] J. B. Mueller, J. Fischer, Y. J. Mange, T. Nann, M. Wegener, *Appl. Phys. Lett.* **2013**, *103*, 123107.
[20] V. Hahn, T. Messer, N. M. Bojanowski, E. R. Curticean, I. Wacker, R. R. Schröder, E. Blasco, M. Wegener, *Nat. Photonics* **2021**, *15*, 932.
[21] J. C. Scaiano, L. J. Johnston, W. G. McGimpsey, D. Weir, *Acc. Chem. Res.* **1988**, *21*, 22.
[22] T. S. Fang, R. E. Brown, C. L. Kwan, L. A. Singer, *J. Phys. Chem.* **1978**, *82*, 2489.
[23] F. Auzel, *Chem. Rev.* **2004**, *104*, 139.
[24] B. Culshaw, J. M. López-Higuera, in *Optochemical Nanosensors*, Wiley, Hoboken, NJ **2016**, 3.
[25] P. J. Wagner, A. E. Kemppainen, H. N. Schott, *J. Am. Chem. Soc.* **1973**, *95*, 5604.
[26] A. Mauri, P. Kiefer Karlsruher, P. Neidinger, T. Messer, N. M. Bojanowski, L. Yang, S. Walden, A.-N. Unterreiner, C. Barner-Kowollik, M. Wegener, W. Wenzel, M. Kozlowska, *Two- and three-photon processes in photoinitiators for 3D laser printing*, Research Square **2022**.
[27] T. Cáceres, M. V. Encinas, E. A. Lissi, *J. Photochem.* **1984**, *27*, 109.
[28] L. J. Johnston, M. Tencer, J. C. Scaiano, *J. Org. Chem.* **1986**, *51*, 2806.
[29] A. S. Tatikolov, V. A. Kuzmin, L. A. Singer, *Chem. Phys. Lett.* **1986**, *124*, 451.
[30] V. Hahn, P. Rietz, F. Hermann, P. Müller, C. Barner-Kowollik, T. Schlöder, W. Wenzel, E. Blasco, M. Wegener, *Nat. Photonics* **2022**, *16*, 784.
[31] A. Singh, A. R. Scott, F. Sopchyshyn, *J. Phys. Chem.* **1969**, *73*, 2633.
[32] M. Regehly, Y. Garmshausen, M. Reuter, N. F. König, E. Israel, D. P. Kelly, C. Y. Chou, K. Koch, B. Asfari, S. Hecht, *Nature* **2020**, *588*, 620.
[33] G. K. Das Mohapatra, J. Bhattacharya, J. Bandopadhyay, S. C. Bera, *J. Photochem.* **1987**, *40*, 47.
[34] E. Frick, C. Schweigert, B. B. Noble, H. A. Ernst, A. Lauer, Y. Liang, D. Voll, M. L. Coote, A. N. Unterreiner, C. Barner-Kowollik, *Macromolecules* **2016**, *49*, 80.
[35] T. J. A. Wolf, D. Voll, C. Barner-Kowollik, A.-N. Unterreiner, *Macromolecules* **2012**, *45*, 2257.
[36] F. Babudri, V. Fiandanese, G. Marchese, A. Punzi, *Tetrahedron Lett.* **1995**, *36*, 7305.
[37] Y. Shimakawa, T. Morikawa, S. Sakaguchi, *Tetrahedron Lett.* **2010**, *51*, 1786.
[38] H. Han, Y. R. Liu, C. Dong, X. en Han, *J. Lumin.* **2017**, *183*, 513.
[39] P. Hoyos, G. Sansottera, M. Fernández, F. Molinari, J. V. Sinisterra, A. R. Alcántara, *Tetrahedron* **2008**, *64*, 7929.
[40] S. W. Kim, T.-W. Um, S. Shin, *J. Org. Chem.* **2018**, *83*, 4703.
[41] A. J. Kay, A. D. Woolhouse, G. J. Gainsford, T. G. Haskell, C. P. Wyss, S. M. Giffin, I. T. McKinnie, T. H. Barnes, *J. Mater. Chem.* **2001**, *11*, 2272.
[42] S. Ruengsangtongkul, N. Chaisan, C. Thongsornkleeb, J. Tummatorn, S. Ruchirawat, *Org. Lett.* **2019**, *21*, 2514.
[43] N. Griebenow, T. Meyer, *Synlett* **2010**, *17*, 2639.
[44] J. W. Ogle, J. Zhang, J. H. Reibenspies, K. A. Abboud, S. A. Miller, *Org. Lett.* **2008**, *10*, 3677.
[45] A. V. Zaytsev, R. Bulmer, V. N. Kozhevnikov, M. Sims, G. Modolo, A. Wilden, P. G. Waddell, A. Geist, P. J. Panak, P. Wessling, F. W. Lewis, *Chem. - Eur. J.* **2020**, *26*, 428.
[46] A. Venkatesh, L. Saatwika, A. Karthick, A. Subbiya, I. Post, *Eur. J. Mol. Clin. Med.* **2020**, *7*, 1245.
[47] L. Horner, F. Maurer, *Justus Liebigs Ann Chem* **1970**, *736*, 145.
[48] R. B. Grubbs, *Polym. Rev.* **2011**, *51*, 104.
[49] Y. Jia, C. A. Spiegel, A. Welle, S. Heißler, E. Sedghamiz, M. Liu, W. Wenzel, M. Hackner, J. P. Spatz, M. Tsotsalas, E. Blasco, *Adv. Funct. Mater.* **2022**, 2207826.
[50] T. Frenzel, M. Kadic, M. Wegener, *Science* **2017**, *358*, 1072.
[51] Y. Tani, M. Terasaki, M. Komura, T. Ogawa, *J. Mater. Chem. C* **2019**, *7*, 11926.
[52] J. Jakubiak, X. Allonas, J. P. Fouassier, A. Sionkowska, E. Andrzejewska, L. Å. Linden, J. F. Rabek, *Polymer* **2003**, *44*, 5219.
[53] L. Yang, A. Münchinger, M. Kadic, V. Hahn, F. Mayer, E. Blasco, C. Barner-Kowollik, M. Wegener, *Adv. Opt. Mater.* **2019**, *7*, 1901040.
[54] N. Liaros, J. T. Fourkas, *Laser Photonics Rev.* **2021**, *15*, 2000203.
[55] K. Schwarzschild, *Astrophys. J.* **1900**, *11*, 89.
[56] D. Holtz, in *Progress in Physical Organic Chemistry*, Wiley, NJ **2007**, 1.
[57] P. L. Verheijdt, H. Cerfontain, *J. Chem. Soc., Perkin Trans. 2* **1982**, *12*, 1541.
[58] P. Müller, R. Müller, L. Hammer, C. Barner-Kowollik, M. Wegener, E. Blasco, *Chem. Mater.* **2019**, *31*, 1966.
[59] J. Fischer, M. Wegener, *Adv. Mater.* **2012**, *24*, OP65.
[60] T. J. A. Wolf, J. Fischer, M. Wegener, A.-N. Unterreiner, *Opt. Lett.* **2011**, *36*, 3188.
[61] J. Fischer, J. B. Mueller, A. S. Quick, J. Kaschke, C. Barner-Kowollik, M. Wegener, *Adv. Opt. Mater.* **2015**, *3*, 221.
[62] J. Fischer, M. Wegener, *Opt. Mater. Express* **2011**, *1*, 614.
[63] J. F. Arnett, S. P. McGlynn, *J. Phys. Chem.* **1975**, *79*, 626.
[64] J. P. Malval, C. Dietlin, X. Allonas, J. P. Fouassier, *J. Photochem. Photobiol., A* **2007**, *192*, 66.
[65] T. R. Evans, P. A. Leermakers, *J. Am. Chem. Soc.* **1967**, *89*, 4380.
[66] N. J. Leonard, E. R. Blout, *J. Am. Chem. Soc.* **1950**, *72*, 484.
[67] J. Fischer, G. Von Freymann, M. Wegener, *Adv. Mater.* **2010**, *22*, 3578.
[68] N. Li, R. R. Gattass, E. Gershgoren, H. Hwang, J. T. Fourkas, *Science* **2009**, *324*, 910.